THE JOURNAL OF PHYSICAL CHEMISTRY C

Effect of Swelling on Multiple Energy Transfer in Conjugated Polymer Nanoparticles

Louis C. Groff,[‡] Yifei Jiang,[†] Xiaoli Wang,[§] and Jason D. McNeill*,[†]

[†]Department of Chemistry, Clemson University, Clemson, South Carolina 29634, United States

[‡]Department of Chemistry, Emory University, Atlanta, Georgia 30322, United States

[§]Department of Molecular and Cellular Medicine, Texas A&M University, College Station, Texas 77845, United States

ⓢ *Supporting Information*

ABSTRACT: Many key processes in conjugated polymers are strongly influenced by multiple energy transfer (i.e., exciton diffusion). We investigated the effect of solvent-induced swelling on the kinetics of multiple energy transfer in nanoparticles of the conjugated polymers PFBT and MEH-PPV. Multiple energy transfer between equivalent chromophores results in an increased rate of quenching by defects due to a cascading or funneling effect. The effects of swelling on energy transfer between polymer chromophores and the resulting exciton dynamics were modeled using a random walk on a lattice of chromophores. The simulation results show good agreement with experimental fluorescence quantum yield, and decay kinetics results at low to moderate THF concentrations. We found that the time scale for energy transfer between chromophores (~5 ps for MEH-PPV nanoparticles and ~100 ps for PFBT nanoparticles) is highly sensitive to swelling, slowing by an order of magnitude or more for swelled particles. The results support quenching by defects or polarons, amplified by multiple energy transfer or a cascade effect, as a likely explanation for the typically low fluorescence quantum yield of conjugated polymer particles as compared to the free polymer in solution as well as similar effects observed in thin films.
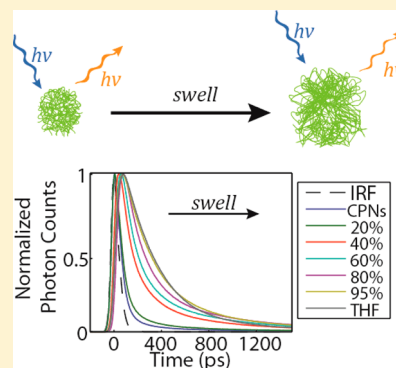
■ INTRODUCTION

Conjugated polymers (CPs) are a versatile class of semi-conducting luminescent materials, used as active materials in organic photovoltaics and light-emitting diodes.[1−3] Conjugated polymer nanoparticles (CPNs) are well-suited to a variety of fluorescence-based imaging and sensing applications, exhibiting extraordinary figures of merit, including exceptional brightness and photostability.[4,5] Furthermore, highly efficient energy transfer to dyes or other polymers incorporated in the particle or to dyes covalently linked to the surface can provide red-shifted emission and sensors.[5−9] To tune CPN properties for various applications, we seek to better understand the species and processes that dictate their properties, and how they are modulated by polymer conformation and processing conditions.[10,11] The complex, nanoscale, multichromophoric nature of CPNs can give rise to a number of transient and persistent species interacting with the excited state including H- or J-aggregates, excimers, and exciplexes.[12−15] Furthermore, chemical defects, excess charges (i.e., hole polarons), and incorporated dyes can have significant effects on fluorescence properties.[16−21] In addition, energy transfer between like conjugated polymer chromophores (i.e., exciton diffusion) can result in a cascade of multiple energy transfer events, greatly amplifying the effects of these species.[22−25] Recently, we showed that multiple energy transfer in CPNs gives rise to characteristic complex fluorescence kinetics.[7]

Here, we investigate the effects of solvent-induced swelling on the excited-state dynamics in CPNs, using steady-state and time-resolved fluorescence spectroscopy to develop and test a multiple energy transfer model and thus gain a clearer picture of the interplay of the various species and processes that determine the optical properties and excited-state dynamics of CPNs. We previously employed a similar approach to determine the length scale of exciton diffusion in dye-doped CPNs.[7] Particle swelling increases the interchromophore distance, causing a reduction in the rate of multiple energy transfer and thus a reduction in the quenching efficiency and an increase in the excited-state lifetime. By fitting parameters of a multiple energy transfer model to picosecond fluorescence decay results, we obtain an approximate picture of the characteristic length scale and time scale of energy transfer between pairs of like chromophores (homotransfer) as well as how the energy transfer cascade is modulated by swelling. The agreement with model predictions over a broad range of swelling supports the proposed multiple energy transfer picture. The comparison of results from two different polymers suggests that higher rates of homotransfer, which are sometimes desired (e.g., to improve exciton transport in photovoltaics, or for some sensor schemes), come at the price of reduced fluorescence

quantum yield due to increased quenching by defects, either due to the formation of additional aggregate species for systems with higher chromophore densities or due to an increase in the energy transfer cascade to pre-existing defects. Our results point to the latter mechanism as the more likely or dominant mechanism causing the large reduction in fluorescence quantum yield often observed for some conjugated polymer films and particles as compared to the free polymer in solution. On the basis of this picture, we suggest that, in some cases, the optical properties CP films and particles can be improved by interfering with the multiple energy transfer cascade, either by competitive energy transfer or by increasing chromophore spacing.

■ EXPERIMENTAL METHODS

Materials. The copolymer poly[(9,9-dioctylfluorenyl-2,7-diyl)-*co*-(1,4-benzo-{2,1′,3}-thiadiazole)] (PFBT, MW 10 000, polydispersity 1.7) and the poly(phenylenevinylene) derivative poly[2-methoxy-5-(2-ethylhexyloxy)-1,4-phenylenevinylene] (MEH-PPV, MW 200 000, polydispersity 4.0) were purchased from ADS Dyes, Inc. (Quebec, Canada). The fluorescent dye fluorescein was purchased from Life Technologies (Invitrogen, Grand Island, NY). The fluorescent dye Lucifer Yellow CH dipotassium salt (LY, 1 mg/mL in water), solvent tetrahydrofuran (THF, anhydrous, inhibitor-free, 99.9%), and sodium hydroxide (SigmaUltra, minimum 98%) were purchased from Sigma-Aldrich (Milwaukee, WI). All materials were used as provided without further purification.

Nanoparticle Preparation. The preparation of fluorescent nanoparticles was performed via a previously described nanoprecipitation method.[26] The conjugated polymers PFBT and MEH-PPV were dissolved in THF by gentle agitation and prepared at a concentration of 1000 ppm. An aliquot of each stock solution was used to prepare precursor solutions at 20 ppm. A 2 mL quantity of a given precursor solution was rapidly added into 8 mL of deionized water under bath sonication at a frequency of 40 kHz and room temperature. Removal of THF was accomplished by the following procedure. Nanoparticle suspensions were placed in a vacuum oven under nitrogen flow for 8 h at room temperature to remove enough THF to prevent bumping during the subsequent vacuum evaporation step. Nitrogen flow was ceased, and samples were evaporated under vacuum in a vacuum oven at room temperature using a two-stage rotary vane pump with a base pressure of ∼10 Torr. The samples were heated at ∼40 °C for 6−7 h to remove most of the remaining THF. The total volume of liquid was typically reduced by 60% during the vacuum evaporation process. A Raoult's Law calculation indicates that <1% THF remains in solution at ∼40% volume loss. No residual THF odor was detected in the aqueous samples. Also, at this point, further evaporation yielded no change in the fluorescence spectrum or quantum yield. We validated this process further by assessing the batch-to-batch reproducibility of the fluorescence spectra, and fluorescence quantum yield of the aqueous nanoparticle samples. Four batches of nanoparticles were prepared using each polymer. The nanoparticle fluorescence spectra were identical in shape and peak emission wavelength for both polymers. The fluorescence quantum yield varied between 4% and 6% for PFBT CPNs, and remained constant at ∼1% for MEH-PPV CPNs. The aqueous samples were vacuum filtered through a glass fiber prefilter to remove larger aggregates and a 0.1 μm PVDF membrane filter (Millipore). The fraction of polymer lost in the filtration process was typically ∼10%, as

measured by UV−vis. The resulting suspensions are clear (not turbid) and stable for months with no visible signs of aggregation.

Swelling Procedure. In addition to nanoparticles in water and polymer in THF, swelled nanoparticle samples were prepared by diluting an aliquot of nanoparticle suspension with the appropriate volume of water, followed by slowly adding THF to produce 3 mL of suspensions with volume ratios of THF/water between 0.2 and 0.95. Each sample was gently agitated to ensure solution homogeneity. The sample absorbance was kept at or under ∼0.05 (∼0.02 for 95% THF). Samples were capped and the headspace purged with nitrogen to limit quenching and photobleaching by O_2 (purging was limited to ∼2 min, to limit loss of THF).

Characterization Methods. UV−vis absorption spectra were acquired using a Shimadzu UV2101PC scanning spectrophotometer with 1 cm quartz cuvettes. Fluorescence spectra and fluorescence quantum yield were measured with a commercial fluorimeter (Quantamaster, Photon Technology International) using 1 cm quartz cuvettes. The size distributions and morphologies of the aqueous nanoparticle samples were measured using atomic force microscopy (AFM). Each sample was prepared on a cleaned glass coverslip via immersion casting in a dilute sample of CPNs for 40 min followed by drying overnight in an enclosed environment. The surface topography was measured on an Ambios Q250 multimode AFM in AC mode. Particle diameters were measured via analysis of particle heights. The effect of swelling on the nanoparticle size distributions of PFBT was measured via dynamic light scattering (DLS) using a Nanobrook Omni (Brookhaven Instruments Corp., Holtsville, NY). Swelled CPN samples were prepared according to the above swelling procedure, with a sample absorbance of ∼0.1 at 450 nm. Further details regarding the DLS measurements are provided in the Supporting Information.

Picosecond fluorescence lifetimes were measured under nitrogen using a home-built setup for time-correlated single photon counting (TCSPC) spectroscopy operating in reverse mode. Frequency doubled pulses (420 nm) from a passively mode-locked Ti:sapphire laser (Coherent Mira 900, 840 nm pulses, ∼150 fs pulsewidth) were used as the excitation source for the nanoparticle samples. Fluorescence was collected perpendicular to the excitation source and passed through a 460 nm long pass filter, and a calcite Glan-Taylor polarizer (Thorlabs, GT10-A) oriented at magic angle (55°) with respect to the vertically polarized excitation. The output of a single photon avalanche photodiode (APD, id Quantique, id100-50) was used as the start timing pulse for a time-to-amplitude converter (TAC, Canberra model 2145), and the output of a fast PIN diode (Thorlabs, DET210) was used as the stop pulse, in a standard reverse-mode configuration.[27,28] The excitation power was attenuated (between ∼300 μW and 1 mW, typ.) to maintain a count rate of ∼400 kHz as measured at the APD. The analog TAC output was digitized using a multichannel analyzer (FastComTec, MCA-3A). Before and after each measurement, an instrument response function (IRF) was measured using scattered excitation light from a dilute suspension of polystyrene microspheres. The width of the IRF was determined to be ∼70 ps (fwhm). Typical peak signal-to-noise ratios (SNR) for each run were between 200:1 (80%−100% THF samples) and 500:1 (IRF and low-mid % THF samples). The reported information was collated from a total of two samples per concentration of THF, and 3−5 runs per

198 sample. Intensity decays were collected for 5–20 min each to
199 obtain the above-mentioned signal-to-noise ratio.

■ RESULTS AND DISCUSSION

201 **Characterization of PFBT and MEH-PPV CPNs.** PFBT
202 and MEH-PPV nanoparticles were prepared via a nano-
203 precipitation method described previously.[26] The chemical
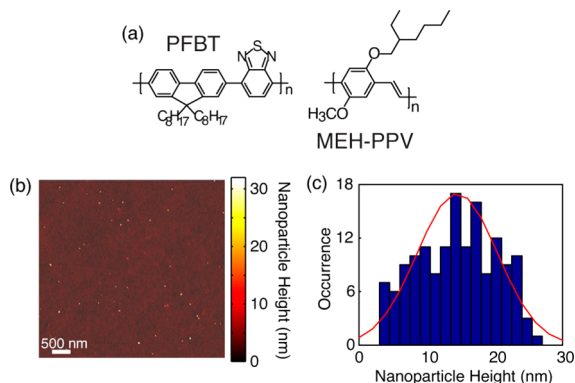204 structures of PFBT and MEH-PPV are given in Figure 1.

Figure 1. (a) Chemical structures of PFBT and MEH-PPV. (b,c) Representative AFM image of PFBT CPNs with particle height histogram.

205 Nanoparticle size distributions were determined via particle
206 height analysis of several AFM images, and each histogram was
207 constructed using >100 particles (cf., Figure 1). The mean
208 particle sizes were 14 ± 6 nm for PFBT CPNs and 9 ± 5 nm
209 for MEH-PPV CPNs, consistent with previous measurements.[5]
210 **Effect of Solvent Composition on UV−Vis and**
211 **Fluorescence.** The UV−vis and fluorescence spectra of
212 PFBT and MEH-PPV as a function of solvent composition
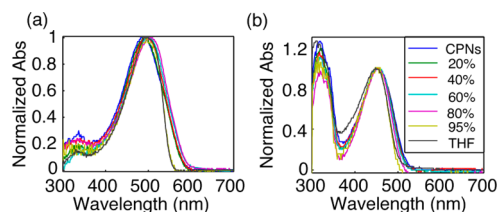213 are given in Figures 2 and 3. The absorption spectra of PFBT

Figure 2. Normalized absorption spectra of (a) MEH-PPV and (b) PFBT at varying volume % THF.

214 maintain a similar shape with increasing THF, with a ∼5 nm
215 total blue shift, and slight broadening of the sample spectrum in
216 100% THF. The emission spectra show a monotonic increase
217 in fluorescence intensity with increasing THF, and the spectra
218 also exhibit a blue shift ∼5 nm with increasing THF. The
219 absorption spectra of MEH-PPV maintain a similar shape as
220 THF concentration is increased, although the 95%−100% THF
221 spectra are narrower than the spectra of the other samples. The
222 absorption peak of MEH-PPV red-shifts a total of ∼15 nm from
223 0%−80% THF, and then blue-shifts ∼7 nm for the 95%−100%
224 THF samples. The emission peak blue-shifts a total of ∼40 nm
225 as THF composition is increased, and it appears that from
226 ∼40% THF to 80% THF there are possibly two phases present
227 in solution based on the increase in intensity of the ∼560 nm
228 shoulder on the spectrum, and the reduction in intensity of the
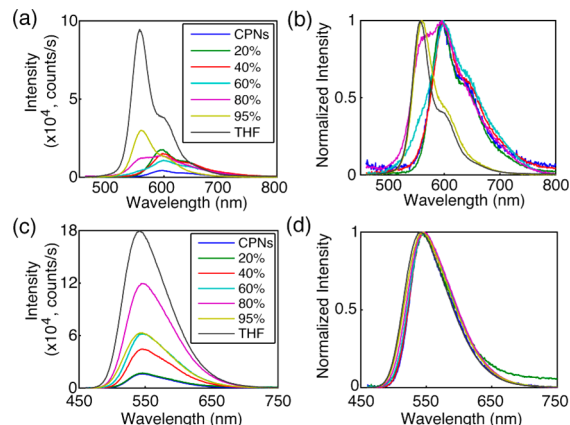229 ∼600 nm shoulder of the spectrum, which correspond to

Figure 3. (a,c) Relative fluorescence intensity as a function of wavelength and (b,d) normalized emission spectra of MEH-PPV (top) and PFBT (bottom) at varying volume % THF.

230 isolated polymer chains and aggregate species, respectively, as
231 % THF increases. A tentative isoemissive point can be seen at
232 ∼580 nm over the concentration range of ∼60%−80% THF.
233 The fluorescence quantum yields (Φ) are given in Figure 4.
234 The quantum yield of PFBT increases monotonically with
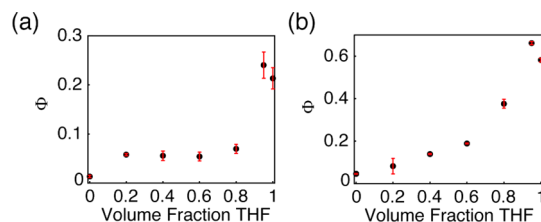
Figure 4. Fluorescence quantum yield versus THF volume fraction for (a) MEH-PPV and (b) PFBT.

235 increasing THF. However, MEH-PPV shows an initial intensity
236 increase from 0%−20% THF, followed by the quantum yield
237 staying relatively consistent from 20% to 80% THF, then
238 increasing at higher % THF. The ∼12% difference in quantum
239 yield between the CPN samples in 95% THF and the dissolved
240 polymers in THF is likely a statistical anomaly due to the
241 uncertainty in the absorbance. While the fluorescence quantum
242 yield remains relatively constant for MEH-PPV from 20% to
243 80% THF, the relative contribution of the ∼600 nm shoulder
244 decreases steadily with increasing THF concentration, likely
245 indicating that this feature is associated with aggregate species.
246 One possible interpretation of the results outlined in Figures
247 3 and 4 is that the coupling between transition dipoles is
248 somewhat stronger for MEH-PPV as compared to PFBT. This
249 is supported by the steady-state spectra, which exhibit a
250 pronounced red-shift in both absorption and emission (for the
251 particles as compared to the polymer dissolved in THF) for
252 MEH-PPV, while PFBT exhibits much smaller shifts. The lesser
253 red shift in the absorption spectra of MEH-PPV as compared to
254 the emission can be explained by a small fraction of highly red-
255 shifted J-aggregate species in conjunction with efficient energy
256 transfer to the aggregate species. This is consistent with the
257 two-state picture of Barbara et al., used to discuss the bimodal
258 emission properties in single molecule spectra of both PFBT
259 and MEH-PPV. In this picture, there is a minority aggregate
260 state that exhibits weak, red-shifted emission, and acts as an
261 energy acceptor to the other (unaggregated) chromo-

phores.[29−33] In the case of swelling, it is likely that swelling either disrupts aggregate formation, or that it reduces the rate of energy transfer to aggregate species, or both.

Picosecond Time-Resolved Fluorescence Spectroscopy. TCSPC obtained at magic angle to the excitation source was employed to measure the excited-state decay kinetics of both CPN systems over the range of solvent composition. The trial functions employed during iterative convolution fitting analysis were single exponential, biexponential, and the Kolrausch−-Williams−Watts (KWW) function or stretched exponential, given by $I(t) = A \exp(-(t/\tau)^\beta)$, where β is the stretch parameter. The run-to-run variability in the obtained fit parameters was less than 10%. Values for β are typically between ∼0.3 and 1, where lower values correspond to a broader distribution of lifetimes, and $\beta = 1$ corresponds to a single exponential lifetime.[34] The fits to all three trial functions converged for all samples. With the exception of PFBT in THF, which was fit best by a single exponential, the remaining intensity decays fit poorly to a single exponential, with the residuals showing systematic deviation consistent with biexponential or multiexponential dynamics. The representative intensity decays for each sample, along with the respective time constants and β versus THF volume fraction, are given in Figure 5. The lifetimes for both systems follow a monotonically

Figure 5. (a,b) Normalized fluorescence intensity decays, and (c,d) lifetimes resulting from single exponential, biexponential weighted average, and KWW trial functions with stretch parameter β (insets) versus THF volume fraction for MEH-PPV and PFBT, respectively.

increasing trend as THF concentration increases. The lifetimes of the CPN samples in water are shorter than previously reported (∼270 ps versus ∼700 ps previously for PFBT), which can be ascribed to a more complete THF removal. This explanation is also consistent with the reduced quantum yield

($\Phi = 0.04$ versus $\Phi = 0.14$ previously for PFBT CPNs).[7] β increases for both systems as the fraction of THF increases, beginning at ∼0.3 for MEH-PPV in water and increasing monotonically to ∼0.8 for MEH-PPV in THF, indicating an overall decrease in lifetime heterogeneity, although even in good solvent there is some heterogeneity. The trends in β are more complex for PFBT, beginning at ∼0.6 for CPNs in water and increasing to ∼0.71 for CPNs in 20% THF, suggesting an initial narrowing of the exciton lifetime distribution, likely due to reduced exciton diffusion. While a net decrease in β is observed from 0.71 in 20% THF to 0.65 in 60% THF, which would suggest a gradual broadening of the exciton lifetime distribution with increased nanoparticle swelling, it is uncertain whether this decreasing trend is statistically significant, and is considered instead to be a plateau around 0.7. We do however observe a substantial decrease in β to ∼0.3 at 80% THF, which is indicative of a dramatic increase in the width of the distribution of exciton lifetimes. This deviation from the trend of increasing β as % THF increases is hypothesized to be due to the presence of two distinct emitting populations with substantially different lifetimes at moderately high % THF, discussed further below. At the highest concentrations of THF, we observe β near unity, indicating that PFBT exists as unassociated chains in solution. While the results at moderate-to-high THF concentrations might seem to be due to spurious artifacts from complex fitting routines to stretched exponential functions, it is worth noting that all of the lifetime dynamics measurements represent the average of six measurements between two distinct samples with under 10% run-to-run variability. The overall trend of increasing β for both polymers is assumed to result from increases in equilibrium chromophore spacing as THF concentration increases, leading to the reduction of the rates of multiple energy transfer to quenchers. This picture is supported by prior results of dye-doped CPNs, where a reduction in β was observed as additional quenchers (dyes) were introduced.[7] The results of the biexponential least-squares fitting analysis are discussed in greater detail below.

A summary of the biexponential least-squares fitting results is given in Table 1. For MEH-PPV, the larger time constant increases monotonically with increasing THF fraction, and the weighted amplitudes do not change appreciably except for MEH-PPV in 100% THF where lifetime is characterized almost entirely by the short time constant. In contrast, the time constants remain approximately the same for PFBT between 80% and 100%, and the weighted amplitude corresponding to the long time constant increases from 80% to 100% THF. Thus, the picosecond kinetics results perhaps suggest a two state-like equilibrium, in which swelled nanoparticles and isolated polymer chains coexist in varying ratios, within a
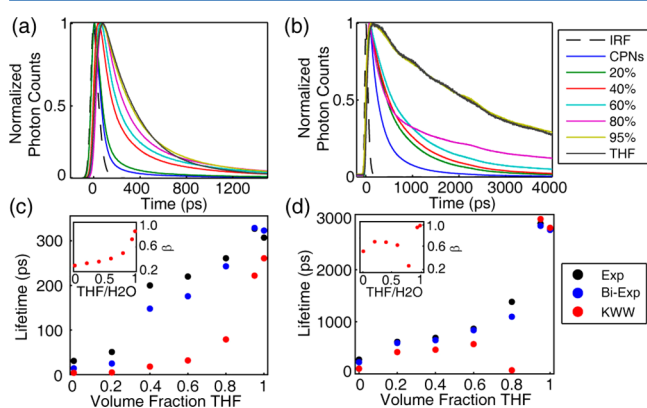
Table 1. Summary of Results of Biexponential Least-Squares Fitting to Time-Resolved Fluorescence of MEH-PPV and PFBT CPNs, Including Weighted Amplitudes (A_1, A_2) and Individual Exponential Time Constants (τ_1, τ_2)

	MEH-PPV				PFBT			
volume fraction THF	A_1	τ_1 (ps)	A_2	τ_2 (ps)	A_1	τ_1 (ps)	A_2	τ_2 (ps)
0	0.96	9	0.04	150	0.59	88	0.41	420
0.20	0.93	14	0.07	180	0.51	260	0.49	940
0.40	0.73	56	0.27	400	0.51	280	0.49	1000
0.60	0.75	74	0.25	480	0.55	360	0.45	1400
0.80	0.75	120	0.25	620	0.65	230	0.35	2700
0.95	0.80	220	0.20	760	0.02	230	0.98	2900
1	0.95	270	0.05	1300	0.01	270	0.99	2800

limited range of THF concentrations. This hypothesis is further supported by the anomalously low β observed for PFBT CPNs in 80% THF and is discussed in more detail below.

Given the red-shifting of fluorescence emission in CPNs relative to the polymers in solution, it is assumed that chain collapse into nanoparticles leads to the formation of J-aggregate species. J-Aggregation is typically accompanied by an increase in radiative rate due to an increase in the net transition dipole moment.[14,35] With this in mind, the radiative rate of a given polymer or CPN sample was calculated using the fluorescence quantum yield and fluorescence lifetime by $k_r = \Phi/\tau_{exp}$. While the uncertainty was too high to observe a clear trend, the radiative rate varied over a factor of ~2 for PFBT (~1.2×10^8 to 2.5×10^8 s^{-1}) and a factor of ~4 (~3.0×10^8 to 1.2×10^9 s^{-1}) for MEH-PPV over the range of THF concentrations, indicating that transition dipole coupling between like chromophores in the nanoparticle phase is possibly stronger in MEH-PPV as compared to PFBT.

Lattice Swelling Model. In a dense, multichromophoric system, (incoherent) exciton transport can be described as a series of energy transfer steps to roughly equivalent neighboring chromophores, terminated by a quencher (e.g., a nonfluorescent chemical defect or red-shifted, weakly fluorescent aggregate), or radiative or nonradiative relaxation to the ground electronic state. The rate of multiple energy transfer depends on the interchromophore spacing, which in the present case is determined by the amount of swelling in the CPNs (i.e., by the solvent composition). Forster's model for exciton diffusion[36] predicts that the exciton diffusion (i.e., multiple energy transfer) rate is increased at high chromophore densities, which in the present case corresponds to low concentrations of the swelling solvent. Furthermore, in the presence of quencher species, increased exciton mobility should result in a higher quenching rate, and increased chromophore density often leads to interchain interactions that give rise to the aforementioned aggregate species. Taken together, these phenomena result in increased quenching and faster decay kinetics in aqueous CPN suspensions as compared to the polymers in good solvent. To test this picture, we have employed a discrete lattice approach using a numerical random walk algorithm to model the effect of solvent-induced swelling on exciton quenching and decay kinetics. Similar approaches were previously utilized to model exciton diffusion and energy transfer in dye-doped nanoparticles on a discrete cubic lattice, and to model fluorescence centroid fluctuations due to polaron motion on single CPNs.[19,20] Here, we represent the particle as a cubic lattice. Each lattice point represents one chromophore, with chromophore spacing determined using the chromophore number density $C_{np} = N_{chorm}/V_{np}$, where N_{chrom} is the approximate number of chromophores per nanoparticle, and V_{np} is the particle volume. We can then determine the chromophore spacing as $\Delta x_{np} = C_{np}^{-1/3} = (V_{np}/N_{chrom})^{1/3}$. Each chromophore is assumed to consist of two monomer units, resulting in a chromophore density (for a 10 nm diameter spherical particle) of $C_{np} = 1.47$ chromophores/nm^3 with chromophore spacing of 0.9 nm for MEH-PPV CPNs, and $C_{np} = 0.61$ chromophores/nm^3 with chromophore spacing of 1.2 nm for PFBT CPNs. This is in the range typically employed for modeling exciton diffusion behavior.[37] Excitons undergo energy transfer between nearest neighbor chromophores (i.e., neighboring lattice sites), and the energy transfer rate is set to reproduce the observed exciton diffusion length from previous work of $L_D = 12$ nm, which is assumed for both

polymers.[7] Treating exciton diffusion as a random walk on a lattice, the probability for a random step in any one direction, in the absence of swelling, is given by $p_{et} = 2D\Delta t/\Delta x_{np}^2$, where Δt is the time step, and D is the exciton diffusion constant given by $D = L_D^2/6\tau_0$, where τ_0 is the lifetime of the polymer in the absence of quenchers. We assume that the quenchers are of the "defect" variety, and do not arise from interchain interactions; thus the average number of defects per nanoparticle is taken as a constant (independent of the degree of swelling). In neglecting the formation of interchain aggregate species as solvent quality decreases, we avoid the problems that arise from attempting to model interchain interactions in this rather complex system. Additionally, we are testing (to some degree) whether aggregate formation is required to explain the results, or if the results can primarily be explained by changes in the rate of energy homotransfer due to swelling.

Swelling of PFBT CPNs in THF/water mixtures was measured by dynamic light scattering (DLS). Below 30% THF, particle radii increased roughly linearly with increasing THF (cf., Supporting Information). At THF ratios above 30%, the particle population splits into multiple populations of both larger and smaller sizes, suggesting a combination of swelling, particle aggregation (forming the larger population fraction), and particle dissociation to form free chains and/or smaller particles at higher THF ratios (cf., Supporting Information). A similar phenomenon was previously reported for PPV oligomer aggregates in THF/water mixtures that when THF percentage increases, the particle size distribution obtained from DLS measurement changes from a simple Gaussian to bimodal.[38] For modeling purposes, we assume that swelling increases chromophore spacing linearly as a function of THF fraction over the whole range of concentration, extrapolating from the DLS results over the range of 0−30% THF. Thus, the modeling results in the range of 30−100% THF are not based on swelled particle size and are included merely to indicate how the model results for fluorescence quantum yield and lifetime vary with chromophore spacing. The particles could become irregular in shape or porous, particularly at the surface, even at low THF concentration, due to the small particle size (and thus large surface-to-volume ratio). Thus, the swelled particle size might yield an overestimate of typical nearest-neighbor chromophore spacing. Therefore, we performed a second set of model calculations, using optical microscopy results from Carson et al. for polystyrene microbeads, which swell somewhat less at a given THF ratio.[39] For example, the swelling of PFBT CPNs is roughly 1.3 times higher than that of polystyrene microbeads at 30% THF. We introduce a swelling factor, which accounts for increases in nanoparticle size as THF concentration increases, given by $f = C_s/C_{np} = V_{np}/V_s$, where C_s is the chromophore density of a swelled nanoparticle, V_{np} is the nanoparticle volume in water, and V_s is the swelled nanoparticle volume. This ratio varies between 0 and 1 where $f = 1$ corresponds to a close-packed nanoparticle or film, and 0 represents a spacing of infinity. With the assumption that swelling decreases chromophore density (increases chromophore spacing), the swelled chromophore spacing becomes defined as $\Delta x_s/\Delta x_{np} = f^{-1/3}$. The model quenching efficiency and β are relatively insensitive to the initial chromophore spacing (tested using 0.8 and 1.5 nm lattice spacing, holding all other parameters constant), provided the homotransfer rate is adjusted to give the same exciton diffusion length, in agreement with previous results.[7] The model exciton lifetime is somewhat more sensitive to the choice of initial lattice spacing, yielding a 20% difference

in lifetime (however, assuming that the homotransfer rate is scaled to reproduce L_D regardless of initial chromophore spacing, an increase in lattice spacing leads to a reduction in k_{et}, which would account for the greater differences in the model lifetime results).

According to the exciton diffusion theory of Förster, the exciton diffusion constant for chromophores on a lattice is given by

$$D = \eta \left(\frac{4\pi C}{3} \right)^{4/3} \frac{R_0^6}{\tau_{fl}} \tag{1}$$

where η is a factor that depends on the molecular details, C is the chromophore density, R_0 is the Förster radius, and τ_{fl} is the lifetime.[36,37] Assuming that the η parameter is insensitive to chromophore spacing, and introducing D_0 as the exciton diffusion constant in the absence of swelling, we obtain

$$D' = D_0 f^{4/3} \tag{2}$$

Combining this with the random walk approach described above, we obtain an adjusted energy transfer probability per time step of

$$p'_{et} = p_{et} (\Delta x_{np} / \Delta x_s)^4 \tag{3}$$

where Δx_{np} and Δx_s are the chromophore lattice spacings for nanoparticles in water and swelled nanoparticles, respectively. On the basis of this expression, the exciton dynamics were modeled as follows. The time step size was adjusted so that prior to increasing the interchromophore spacing, the energy transfer probability was between 1% and 5% per time step (although the results are not appreciably affected by differences in time step for Δt between 1 and 10 ps). An integer number of quenchers were placed randomly on the lattice, each with a Förster-type quenching radius of 4 nm, similar to that of a perylene red dye molecule.[7] The mean number of quenchers per nanoparticle was treated as a fit parameter by adding quenchers until the simulated exciton lifetime approximately reproduces the lifetime of CPNs in water, similar to the approach taken previously for estimating the effect of quenching defects in dye-doped CPNs.[7] The grid spacing of the lattice was calculated for a $10 \times 10 \times 10$ nm cubic particle, with the number of grid points given by $N_{grid} = C_{np} d_{np}^3 \approx (d_{np}/\Delta x_{np})^3$, where d_{np} is the particle diameter, resulting in 1331 grid points for MEH-PPV and 512 grid points for PFBT, in the absence of swelling. The fit procedure yielded 10 quenchers (in terms of dye equivalents) on average per NP. The greater number of quenchers per CPN than those previously reported for dye-doped PFBT CPNs (2.2 per CPN) can be ascribed primarily to the fact that a larger particle was assumed in this model. In addition, the Poisson distribution of quenchers has not been accounted for this model, which likely results in somewhat higher values for β (i.e., less lifetime heterogeneity) than previously reported. We neglected to include the effect of Poisson statistics on the system because the effect is likely small for the present system (discussed below). We have discussed the effect of the Poisson distribution of quenchers in detail in our previous work on dye-doped PFBT CPNs.[7]

50 000 random exciton trajectories were calculated using parameters as described above, for each lattice spacing corresponding to 0−100% THF ($f = 1$ to $f = 0.18$), and the quenching efficiencies determined and decay kinetics fit to obtain time constants and β parameters (cf., Figures 6 and 7). At low to moderate THF concentrations, the model results
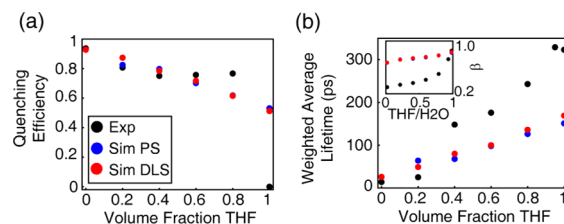

Figure 6. Comparison of simulated (blue, red) and experimental (black) (a) quenching efficiency, (b) average lifetime, and (inset) KWW stretch parameter β versus THF volume fraction for MEH-PPV.
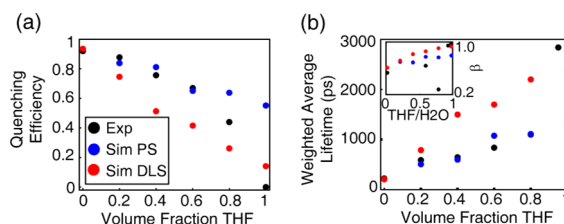

Figure 7. Comparison of simulated (blue, red) and experimental (black) (a) quenching efficiency, (b) average lifetime, and (inset) KWW stretch parameter β versus THF volume fraction for PFBT.

match well to experimental intensity decay kinetics and quenching efficiency, the latter given by $\eta_{exp} = 1 - (\Phi_s / \Phi_{poly})$, where Φ_s and Φ_{poly} are the fluorescence quantum yields of the sample and the polymer in THF, respectively. The simulated quenching efficiency matches the experiment well up to 60% THF for PFBT, and up to 80% THF for MEH-PPV. The time constants obtained from the simulated intensity decays match experimental TCSPC fitting results well up to 20% THF for MEH-PPV and up to 80% THF for PFBT. With the exception of CPNs in 80% THF, β is reproduced relatively well for PFBT. However, β is not reproduced very well for MEH-PPV, except for MEH-PPV in THF (cf., Figure 7). The divergence between simulation and experiment outside of the aforementioned solvent compositions is expected, given that within the regions of moderate THF composition (where particle size increases resulting from swelling are nonlinear), the DLS results suggest a complex mixture of swelling, aggregation, and chain dissociation, particularly between 40% and 80% THF. The poor agreement with experimental β values for MEH-PPV is hypothesized to be due to the exclusion of correlated chromophore orientations and the Poisson distribution of quenchers in this model. Additionally, emission from a longer-lived aggregate state with charge transfer character or a partially oxidized species could be contributing to the complexity of the fluorescence decay.[13,40−42] Given that the model kinetics match experimental decay kinetics well at low THF concentrations, the approximate k_{et} for CPNs in water was calculated from the model energy transfer probabilities by $p_{et} = 1 - \exp(-k_{et}\Delta t)$. The results of these calculations yield model energy transfer rate constants of 2.0×10^{11} s^{-1} (corresponding to a time scale of roughly 5 ps) for MEH-PPV CPNs and 1.1×10^{10} s^{-1} (corresponding to a time scale of roughly 90 ps) for PFBT CPNs, which decreases (slows) monotonically by an order of magnitude over the range of THF composition.

In this and previous work, it has been hypothesized that the reduced quantum yield, reduced fluorescence lifetime, and heterogeneous dynamics of CPNs relative to polymer in good solvent arise from quenching by chemical defects and/or hole

polarons (which may result from oxidation or photogenera-tion).[7] With the assumption that multiple energy transfer is a FRET-mediated process, it follows that the energy transfer efficiency to defect sites would depend upon the number of nearest neighbor chromophores, which is related to the (effective) dimensionality of the system. As an alternate perspective to the above lattice model calculations, the effect of dimensionality on quenching efficiency was investigated (using the PFBT parameters), by determining how quenching efficiency differs in isolated, one-dimensional chains of chromophores versus a 3D spherical particle.

The information for a spherical particle is taken from the above experimental and simulated data for PFBT, in which the particle is assumed to be 10 nm in diameter, with quenching efficiency ~92%. The quenching radius R_q is taken from the simulations at 4 nm. For the one-dimensional case, an ensemble of isolated linear chains is assumed, and the approximate integer number of chains per CPN (N_{chain}) is calculated from the relevant information for a spherical particle. The contour length of each chain is given by $L_{chain} = L_c N_c$, where L_c is the 1D length of one chromophore (assuming C−C bond lengths similar to benzene, yields ~2.5 nm/chromophore), and N_c is the number of chromophores per chain. A number of Poisson distributed quenchers N_q are assumed whose quenching radii do not overlap. The total quenched contour length is calculated by

$$L_q = \sum_{n=0}^{N_q} 2nR_q f_n \qquad (4)$$

where the index n corresponds to the number of quenchers, the fraction of chains in the ensemble containing n Poisson distributed quenchers $f_n = N_n/N_{chain}$, where N_n is the number of chains containing n Poisson distributed quenchers, and quenching efficiency η_{sim} is calculated by

$$\eta_{sim} = L_q/L_{chain} \qquad (5)$$

Equation 2 results in ~11% quenching efficiency for a one-dimensional ensemble of PFBT chains, which supports the notion that even with the same quantity of quenchers in the system, quenching is greatly suppressed as the nanoparticle dissociates into free chains in solution. This also supports one assumption of our quenching picture for CPNs: that quenching by defects is greatly reduced in isolated, extended chains due to a drastic reduction in the rate of multiple energy transfer, which stems largely from the reduced number of nearest neighbor chromophores available for energy transfer in the 1D case, as compared to the 3D case (two neighbors in 1D, versus six neighbors in 3D). This is reflected in the model results, as Förster exciton diffusion theory predicts the reduction of the energy homotransfer rate by an order of magnitude at the highest concentrations of swelling solvent. However, as is shown by the divergence of the model quenching efficiency and decay kinetics to the experimental results at high swelling solvent ratios, even an order of magnitude reduction in the rate of energy transfer is insufficient to accurately model the reduction in quenching efficiency and fluorescence decay rates for high THF ratios. Our proposed picture is further supported by previous modeling of linear polyenes by Beljonne et al., which shows that interchain exciton coupling weakens with increasing intermolecular separation, and as the chain length becomes larger than the intermolecular separation. In addition, it was shown that the magnitude of the intrachain transition

dipole is increased with increasing chain length.[43] Thus, as a particle swells and collapsed chains unfold, the excitonic coupling to interchain nearest neighbors is decreased, disfavoring 2D or 3D exciton transport, and the coupling to intrachain nearest neighbors increases, which favors 1D exciton transport.

Throughout these experiments, there have been several results that suggest that solvent-induced swelling can result in a two-state system at moderate THF concentrations. Biexponen-tial lifetime analysis results for both polymers at moderate THF concentrations yield short time constants similar to the CPNs in water, and long time constants similar to the free polymer in THF. These time constants hold fixed for PFBT from 80% to 95% THF, only shifting in the weighted amplitudes of each (cf., Table 1). The model results also significantly deviate from what is observed experimentally in the region of THF concentration where these phenomena are observed. Taking the lifetime measurements together with the complexity of the swelling results obtained via DLS, it follows that the lattice swelling picture alone is insufficient to describe the physics of the CPNs for moderate to high THF compositions, and it is likely that modeling of nanoparticle dissociation in conjunction with the lattice swelling model would result in better agreement. Additionally, the observed quenching of the polymer fluorescence in aqueous solution can be ascribed to an increased rate of homotransfer from a majority of highly fluorescent, higher energy chromophores to a weakly fluorescent, red-shifted minority of aggregates that act as energy acceptors for both PFBT and MEH-PPV.[31−33] Addi-tionally, steady-state fluorescence results show the red-shifted spectral signatures of the nanoparticle phase in addition to the free (unassociated) polymer spectrum in moderately swelled MEH-PPV samples, and DLS results indicate that multiple populations both large and small exist at moderate-to-high THF ratios, which indicate that unassociated chains in addition to swelled particles and/or large aggregates are likely to coexist at these THF ratios.

We hypothesize that a key contributing factor to the observed differences in the fluorescence lifetimes and quantum yields of PFBT and MEH-PPV nanoparticles is the difference in the rates of multiple energy transfer (i.e., energy homotransfer or exciton diffusion). Both the absorption and the emission spectra of MEH-PPV exhibit significantly larger red-shifts upon particle formation as compared to PFBT, consistent with stronger transition dipole coupling for MEH-PPV, according to exciton theory. Stronger transition dipole coupling is typically associated with a higher rate of energy transfer. Within the lattice energy transfer model, a higher rate of energy transfer between chromophore sites results in an overall higher quenching rate (i.e., reduced fluorescence lifetime) and reduced fluorescence quantum yield, so, according to the model, the higher multiple energy transfer rate of MEH-PPV should result in a more pronounced reduction in fluorescence quantum yield and in fluorescence lifetime for the nanoparticle as compared to the free polymer in solution, whereas PFBT should exhibit a more modest reduction in fluorescence quantum yield and in fluorescence lifetime for the nanoparticle as compared to the free polymer in solution. Indeed, this is what is observed in the experimental results. Thus, for applications that require high exciton mobility (e.g., for photovoltaics, which typically require efficient transport of excitons to a heterojunction), there is a trade-off in that any increase in exciton mobility would also lead

to an increase in the rate of quenching by defects such as hole polarons.

Additionally, we seek to address the question of whether "interchain aggregates" are required to explain the differences between the optical properties of CP in solution versus in films and particles. While in some cases, there is some evidence for possible interchain aggregate species (for example, the highly red-shifted emission of MEH-PPV films and particles), the decay kinetics of the fluorescent excited state are roughly consistent with model results that do not include formation of weakly fluorescent aggregates. This model is based on a picture in which the number of quenching defects in a particle is not dependent on the degree of swelling (e.g., oxidized defects), and that the effective number of chromophores quenched per defect increases as the chromophore density increases, due to the highly sensitive dependence of exciton diffusion length on interchromophore spacing. While this work does not rule out any increased quenching effect due to interchain aggregate species, it does lend some support to an alternative mechanism that could explain the differences between the spectroscopic properties of conjugated polymers in solution as compared to films or particles.

■ CONCLUSION

Amplified quenching due to a multiple energy transfer cascade in PFBT and MEH-PPV conjugated polymer nanoparticles was investigated by measuring the effect of solvent-induced swelling (and the resulting decrease in chromophore density) on the steady-state absorption and fluorescence spectra and fluorescence lifetimes. The lifetime results indicate substantial dynamic quenching at higher chromophore densities (i.e., at lower fractions of THF), consistent with either a combination of distance-dependent multiple energy transfer between polymer chromophores (exciton diffusion) and quenching by defects or, alternatively, formation of nonfluorescent aggregates at lower fractions of THF. Nanoparticle lattice model simulations of multiple energy transfer give results consistent with the experimental results for CPNs in water, indicating that, because of the multiple energy transfer cascade, a quencher density of as low as roughly 1 defect per ~100 chromophores can result in a factor of 10 decrease in excited-state lifetime and a factor of 16 decrease in fluorescence quantum yield. Previous results indicate that hole polarons are likely the primary quenching defect, and are likely present at sufficient densities to account for the observed quenching, assuming a multiple energy transfer cascade. The addition of swelling to the lattice model, assuming that the rate of energy transfer between neighboring chromophores depends on the interchromophore distance to the minus sixth power, in accordance with Förster energy transfer, qualitatively matches the experimental results on moderately swelled CPNs, providing further evidence of multiple energy transfer involving a Förster-like mechanism or other mechanism with similarly strong distance dependence. Furthermore, the results of the lattice model (assuming ~1 nm chromophore spacing) suggest that energy transfer between nearby chromophores occurs on a time scale of roughly 5−90 ps.

At higher THF solvent fractions, there is likely a point at which the nanoparticles dissociate to form free polymer chains; thus the effect of dimensionality (i.e., chain versus particle) on quenching via multiple energy transfer was investigated. A straightforward calculation of quenching in a linear chain of chromophores, assuming similar energy transfer parameters and quencher density, resulted in orders of magnitude reduction in quenching rate and quenching efficiency as compared to the three-dimensional (nanoparticle) lattice model results. This provides some justification for our prior assumption that the fluorescence lifetime of the polymer dissolved in good solvent is largely free of quenching by defects,[7] and matches the swelling results, which are consistent with the onset of particle dissociation into unassociated chains and/or smaller particles at roughly 40% THF, as measured by dynamic light scattering.

On the basis of the swelling results, we posit that the differences between the fluorescence quantum yields and lifetimes of various conjugated polymers are often largely dictated by the strength of coupling between (like) chromophores and thus the rate of multiple energy transfer. In other words, materials with higher exciton mobility exhibit more quenching via an energy transfer cascade to chemical defects or other quenching species (e.g., hole polarons), and thus tend to exhibit shorter fluorescence lifetimes and reduced fluorescence quantum yield. On the basis of our observations, we consider it likely that the much lower fluorescence lifetime and quantum yield of MEH-PPV CPNs relative to PFBT CPNs could be largely due to differences in exciton mobility. This amplified quenching effect could give rise to trade-offs in applications requiring both high fluorescence quantum yield (or long exciton lifetime) and high exciton mobility, such as in organic photovoltaic devices and CPN sensors.

■ ASSOCIATED CONTENT

⑤ Supporting Information

The Supporting Information is available free of charge on the ACS Publications website at DOI: 10.1021/acs.jpcc.7b00892.

Procedures of CPNs preparation and characterization, information on dynamics light scattering measurement, determination of fluorescence quantum yield, and information on fluorescence lifetime measurement (PDF)

■ AUTHOR INFORMATION

Corresponding Author
*E-mail: mcneill@clemson.edu.

ORCID Ⓘ
Jason D. McNeill: 0000-0003-2568-8174

Notes
The authors declare no competing financial interest.

■ ACKNOWLEDGMENTS

■ REFERENCES

(1) Dennler, G.; Sariciftci, N. S. Flexible Conjugated Polymer-Based Plastic Solar Cells: From Basics to Applications. *Proc. IEEE* **2005**, *93* (8), 1429−1439.

(2) Yim, K. H.; Zheng, Z.; Liang, Z.; Friend, R. H.; Huck, W. T. S.; Kim, J. S. Efficient Conjugated-Polymer Optoelectronic Devices Fabricated by Thin-Film Transfer-Printing Technique. *Adv. Funct. Mater.* **2008**, *18*, 1012−1019.

(3) Cao, Y.; Parker, I. D.; Yu, G.; Zhang, C.; Heeger, A. J. Improved Quantum Efficiency for Electroluminescence in Semiconducting Polymers. *Nature* **1999**, *397*, 414−417.

(4) Wu, C. F.; Bull, B.; Szymanski, C.; Christensen, K.; McNeill, J. Multicolor Conjugated Polymer Dots for Biological Fluorescence Imaging. *ACS Nano* **2008**, *2* (11), 2415−2423.

805 (5) Wang, X. L.; Groff, L. C.; McNeill, J. D. Photoactivation and
806 Saturated Emission in Blended Conjugated Polymer Nanoparticles.
807 *Langmuir* **2013**, *29* (45), 13925−13931.

808 (6) Wu, C. F.; Peng, H.; Jiang, Y.; McNeill, J. Energy Transfer
809 Mediated Fluorescence from Blended Conjugated Polymer Nano-
810 particles. *J. Phys. Chem. B* **2006**, *110*, 14148−14154.

811 (7) Groff, L. C.; Wang, X. L.; McNeill, J. D. Measurement of Exciton
812 Transport in Conjugated Polymer Nanoparticles. *J. Phys. Chem. C*
813 **2013**, *117* (48), 25748−25755.

814 (8) Chan, Y. H.; Wu, C. F.; Ye, F. M.; Jin, Y. H.; Smith, P. B.; Chiu,
815 D. T. Development of Ultrabright Semiconducting Polymer Dots for
816 Ratiometric PH Sensing. *Anal. Chem.* **2011**, *83* (4), 1448−1455.

817 (9) Childress, E. S.; Roberts, C. A.; Sherwood, D. Y.; LeGuyader, C.
818 L.; Harbron, E. J. Ratiometric Fluorescence Detection of Mercury Ions
819 in Water by Conjugated Polymer Nanoparticles. *Anal. Chem.* **2012**, *84*
820 (3), 1235−1239.

821 (10) Schaller, R. D.; Snee, P. T.; Johnson, J. C.; Lee, L. F.; Wilson, K.
822 R.; Haber, L. H.; Saykally, R. J.; Nguyen, T. Q.; Schwartz, B. J.
823 Nanoscopic Interchain Aggregate Domain Formation in Conjugated
824 Polymer Films Studied by Third Harmonic Generation Near-Field
825 Scanning Optical Microscopy. *J. Chem. Phys.* **2002**, *117* (14), 6688−
826 6698.

827 (11) Wu, C. F.; McNeill, J. Swelling-Controlled Polymer Phase and
828 Fluorescence Properties of Polyfluorene Nanoparticles. *Langmuir*
829 **2008**, *24* (11), 5855−5861.

830 (12) Nguyen, T. Q.; Doan, V.; Schwartz, B. J. Conjugated Polymer
831 Aggregates in Solution: Control of Interchain Interactions. *J. Chem.*
832 *Phys.* **1999**, *110* (8), 4068−4078.

833 (13) Jenekhe, S. A.; Osaheni, J. A. Excimers and Exciplexes of
834 Conjugated Polymers. *Science* **1994**, *265* (5173), 765−768.

835 (14) Wurthner, F.; Kaiser, T. E.; Saha-M?ller, C. R.; J-Aggregates.
836 From Serendipitous Discovery to Supramolecular Engineering of
837 Functional Dye Materials. *Angew. Chem., Int. Ed.* **2011**, *50* (15), 3376−
838 3410.

839 (15) Jakubiak, R.; Collison, C. J.; Wan, W. C.; Rothberg, L. J.; Hsieh,
840 B. R. Aggregation Quenching of Luminescence in Electroluminescent
841 Conjugated Polymers. *J. Phys. Chem. A* **1999**, *103* (14), 2394−2398.

842 (16) Hintschich, S. I.; Rothe, C.; Sinha, S.; Monkman, A. P.; de
843 Freitas, P. S.; Scherf, U. Population and Decay of Keto States in
844 Conjugated Polymers. *J. Chem. Phys.* **2003**, *119* (22), 12017−12022.

845 (17) Yu, J.; Song, N. W.; McNeill, J. D.; Barbara, P. F. Efficient
846 Exciton Quenching by Hole Polarons in the Conjugated Polymer
847 MEH-PPV. *Isr. J. Chem.* **2004**, *44* (1−3), 127−132.

848 (18) Lyons, B. P.; Monkman, A. P. The Role of Exciton Diffusion in
849 Energy Transfer between Polyfluorene and Tetraphenyl Porphyrin.
850 *Phys. Rev. B: Condens. Matter Mater. Phys.* **2005**, *71*, 235201−235205.

851 (19) Wu, C. F.; Zheng, Y. L.; Szymanski, C.; McNeill, J. Energy
852 Transfer in a Nanoscale Multichromophoric System: Fluorescent Dye-
853 Doped Conjugated Polymer Nanoparticles. *J. Phys. Chem. C* **2008**,
854 *112*, 1772−1781.

855 (20) Yu, J.; Wu, C. F.; Tian, Z.; McNeill, J. Tracking of Single Charge
856 Carriers in a Conjugated Polymer Nanoparticle. *Nano Lett.* **2012**, *12*,
857 1300−1306.

858 (21) Gesquiere, A. J.; Park, S.-J.; Barbara, P. F. Hole-Induced
859 Quenching of Triplet and Singlet Excitons in Conjugated Polymers. *J.*
860 *Am. Chem. Soc.* **2005**, *127* (26), 9556−9560.

861 (22) Scholes, G. D. Rumbles, G. Excitons in Nanoscale Systems. *Nat.*
862 *Mater.* **2006**, *5*, 683−696.

863 (23) Kasha, M. Energy Transfer Mechanisms and the Molecular
864 Exciton Model for Molecular Aggregates. *Radiat. Res.* **1963**, *20* (1),
865 55−70.

866 (24) Mikhnenko, O. V.; Blom, P. V. M; Nguyen, T. Q. Exciton
867 Diffusion in Organic Semiconductors. *Energy Environ. Sci.* **2015**, *8*
868 (Advance Article), 1−22.

869 (25) Jiang, Y.; McNeill, J. Light-Harvesting and Amplified Energy
870 Transfer in Conjugated Polymer Nanoparticles. *Chem. Rev.* **2017**, *117*
871 (2), 838−859.

872 (26) Szymanski, C.; Wu, C. F.; Hooper, J.; Salazar, M. A.; Perdomo,
873 A.; Dukes, A.; McNeill, J. Single Molecule Nanoparticles of the
874 Conjugated Polymer MEH-PPV, Preparation and Characterization by
875 Near-Field Scanning Optical Microscopy. *J. Phys. Chem. B* **2005**, *109*,
876 8543−8546.

877 (27) Schaffer, J.; Volkmer, A.; Eggeling, C.; Subramaniam, V.; Striker,
878 G.; Seidel, C. A. M. Identification of Single Molecules in Aqueous
879 Solution by Time-Resolved Fluorescence Anisotropy. *J. Phys. Chem. A*
880 **1999**, *103* (3), 331−336.

881 (28) Cross, A. J.; Fleming, G. R. Analysis of Time-Resolved
882 Fluorescence Anisotropy Decays. *Biophys. J.* **1984**, *46* (1), 45−56.

883 (29) Yu, J.; Hu, D. H.; Barbara, P. F. Unmasking Electronic Energy
884 Transfer of Conjugated Polymers by Suppression of O₂ Quenching.
885 *Science* **2000**, *289* (5483), 1327−1330.

886 (30) Yip, W. T.; Hu, D. H.; Yu, J.; Vanden Bout, D. A.; Barbara, P. F.
887 Classifying the Photophysical Dynamics of Single- and Multiple-
888 Chromophoric Molecules by Single Molecule Spectroscopy. *J. Phys.*
889 *Chem. A* **1998**, *102* (39), 7564−7575.

890 (31) Grey, J. K.; Kim, D. Y.; Donley, C. L.; Miller, W. L.; Kim, J. S.;
891 Silva, C.; Friend, R. H.; Barbara, P. F. Effect of Temperature and Chain
892 Length on the Bimodal Emission Properties of Single Polyfluorene
893 Copolymer Molecules. *J. Phys. Chem. B* **2006**, *110* (38), 18898−18903.

894 (32) Lee, Y. J.; Kim, D. Y.; Barbara, P. F. Effect of Sample
895 Preparation and Excitation Conditions on the Single Molecule
896 Spectroscopy of Conjugated Polymers. *J. Phys. Chem. B* **2006**, *110*
897 (20), 9739−9742.

898 (33) Kim, D. Y.; Grey, J. K.; Barbara, P. F. A Detailed Single
899 Molecule Spectroscopy Study of the Vibronic States and Energy
900 Transfer Pathways of the Conjugated Polymer MEH-PPV. *Synth. Met.*
901 **2006**, *156* (2−4), 336−345.

902 (34) Chen, R. Apparent Stretched-Exponential Luminescence Decay
903 in Crystalline Solids. *J. Lumin.* **2003**, *102*, 510−518.

904 (35) Jelley, E. E. Molecular, Nematic and Crystal States of I: I-
905 Diethyl–Cyanine Chloride. *Nature* **1937**, *139*, 631−632.

906 (36) Förster, T. Intermolecular Energy Migration and Fluorescence.
907 *Ann. Phys.* **1948**, *437*, 55−75.

908 (37) Bardeen, C. J. The Structure and Dynamics of Molecular
909 Excitons. *Annu. Rev. Phys. Chem.* **2014**, *65*, 127−148.

910 (38) So, W. Y.; Hong, J.; Kim, J. J.; Sherwood, G. A.; Chacon-Madrid,
911 K.; Werner, J. H.; Shreve, A. P.; Peteanu, L. A.; Wildeman, J. Effects of
912 Solvent Properties on the Spectroscopy and Dynamics of Alkoxy-
913 Substituted PPV Oligomer Aggregates. *J. Phys. Chem. B* **2012**, *116*
914 (35), 10504−10513.

915 (39) Lee, J. H.; Gomez, I. J.; Sitterle, V. B.; Meredith, J. C. Dye-
916 Labeled Polystyrene Latex Microspheres Prepared via a Combined
917 Swelling-Diffusion Technique. *J. Colloid Interface Sci.* **2011**, *363* (1),
918 137−144.

919 (40) Yan, M.; Rothberg, L. J.; Papadimitrakopoulos, F.; Galvin, M. E.;
920 Miller, T. M. Defect Quenching of Conjugated Polymer Lumines-
921 cence. *Phys. Rev. Lett.* **1994**, *73* (5), 744−747.

922 (41) Yan, M.; Rothberg, L. J.; Kwock, E. W.; Miller, T. M. Interchain
923 Excitations in Conjugated Polymers. *Phys. Rev. Lett.* **1995**, *75* (10),
924 1992−1995.

925 (42) Papadimitrakopoulos, F.; Konstadinidis, K.; Miller, T. M.; Opila,
926 R.; Chandross, E. A.; Galvin, M. E. The Role of Carbonyl Groups in
927 the Photoluminescence of Poly(p-phenylenevinylene). *Chem. Mater.*
928 **1994**, *6*, 1563−1568.

929 (43) Beljonne, D.; Cornil, J.; Silbey, R.; Millié, P.; Bredás, J. L.
930 Interchain Interactions in Conjugated Materials: The Exciton Model
931 versus the Supermolecular Approach. *J. Chem. Phys.* **2000**, *112* (10),
932 4749−4758.